32^{nd} *URSI GASS, Montreal, 19-26 August 2017*

A Planar Controlled Reception Pattern Array with Dual-Mode TM_{11}-TM_{21} Microstrip Antenna Elements for Increased Angular Coverage

Navid Rezazadeh* (1) and Lotfollah Shafai (1)
(1) University of Manitoba, Winnipeg, MB, Canada R3T5V6
rezazadn@myumanitoba.ca
Lot.Shafai@umanitoba.ca

Abstract

A planar controlled reception pattern array (CRPA) with increased upper hemisphere angular coverage is designed and studied. The array consists of three dual-mode TM_{11}-TM_{21} circular microstrip elements. The TM_{11} patch is circularly polarized (CP) while the TM_{21} patch is dual polarized to exploit more degrees of freedom. The nulling performance of the array is studied using a Monte Carlo approach and is benchmarked against a uniform circular array (UCA) of TM_{11} elements and a spherical array. It is shown that for low elevation angle RFIs, the proposed array provides more angular space available for reception, compared to the planar UCA.

1. Introduction

The global navigation satellite system (GNSS) receivers are vulnerable to radio frequency interference (RFI) and multipath in the environment. Controlled reception pattern arrays (CRPAs) are one of the most robust means of suppressing RFIs [1]. Such arrays allow for realization of a spatial filter to steer nulls of the radiation pattern at RFI angles and form maximum beams towards the satellites. The spatial filter is implemented by multiplying the signals received at each port of the array by complex weights which are updated adaptively.

Microstrip antenna (MSA) arrays are a suitable choice for such arrays due to their low profile and relatively easy fabrication procedure. Planar MSA arrays however have degraded angular availability when nulling low elevation angle RFIs [2], i.e. the angular space with an acceptable signal-to-interference-and-noise (SINR) at the output of the adaptive array is diminished. This is an important issue since the reception from low elevation angle satellites is necessary for a better dilution of precision (DOP) and thus an accurate position-velocity-time (PVT) solution [3]. Curved and non-planar arrays have been suggested and shown to address this issue [2,4] since the array curvature helps to increase the available gain at low elevation angles. They are however bulky and not as easy to produce as planar arrays.

In this work, we investigate the use of a second order azimuthal mode of circular MSAs, TM_{21}, to improve the angular availability of a planar array. An array with λ_0 diameter, consisting of dual-mode TM_{11}-TM_{21} MSA elements is designed at the GPS L1 frequency band, fabricated and measurement results are given in section 2. The nulling performance of the array is studied and compared to a uniform circular array (UCA) and a spherical array in section 3.

2. Array Geometry and Antenna Parameters

The geometry of the antenna array is shown in Figure 1 (a). There are three dual-mode TM_{11}-TM_{21} elements each with three coaxial probes. Slits are cut in the substrate and the ground plane between adjacent elements to reduce the coupling levels. A single element's geometry, which is based on the design in [5], is shown in Figure 1 (b). It consists of an outer shorted ring patch working in TM_{21} mode and an inner TM_{11} circular patch. An oval slit is cut in the TM_{11} patch and it is fed at 45° for RHCP radiation with a single probe. The outer ring is fed by two coaxial probes at 135° to excite two orthogonal polarizations.

The array which is fed by a total of nine coaxial ports has eight degrees of freedom to null RFIs. Furthermore, the patches excluding the ground plane fit into a circle with a diameter of λ_0 at the GPS L1 center frequency.

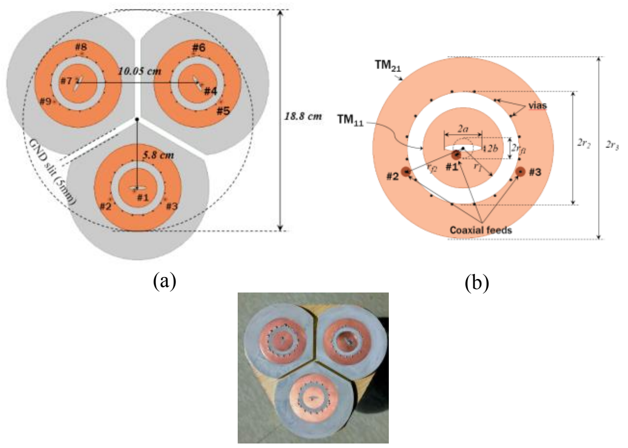

(a) (b) (c)

Figure 1. An array consisting of three TM_{11}-TM_{21} elements, with a total of nine ports. (a) Array geometry. (b) Fabricated array. (c) Geometry of a single element.

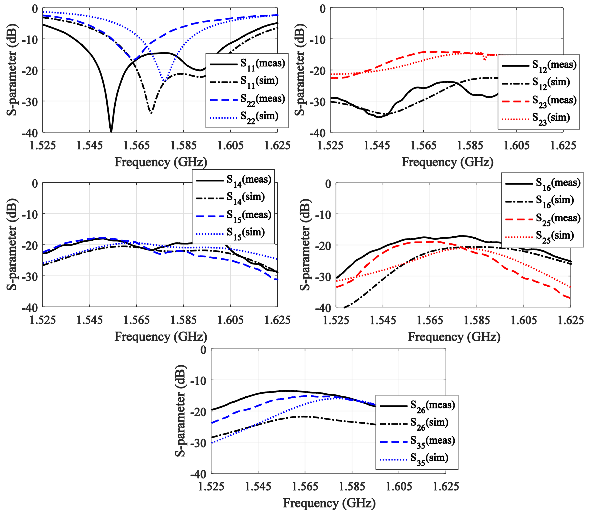

Figure 2. The simulated and measured S-parameters of the array shown in Fig. 1. The ports are labeled as shown in Fig. 1 (a).

The simulated (in HFSS) and measured scattering parameters of the antenna are shown in Figure 2. The frequency shift between the two sets of results is due to the inaccurate estimate of the substrate permittivity in simulation. The coupling levels between the ports remains below -13.5 dB.

The element radiation pattern was measured in a spherical near field range and the normalized amplitudes are shown in Figure. 3. The results are given for only port 1 and 2, since the other ports are similar due to the symmetry in the geometry of the array. The TM_{11} patch (port 1) has a broadside RHCP pattern with the maximum at zenith while the TM_{21} patch (port 2) has a null at zenith and an azimuthal periodicity in the pattern that is consistent with the general form of the radiated fields of a circular MSA at its second azimuthal mode.

The measured realized gain of the TM_{11} and TM_{21} patches are 6 dBic and 2 dBi respectively, which are adequate for GNSS application. The measured radiation patterns are used in the next section to evaluate the nulling performance of the array.

3. Array Null-Steering Performance

To evaluate the nulling performance of the array, the power minimization method subject to a linear constraint is adopted to find the adaptive array weights in steady state. Only the narrowband case is considered where all signals are continuous wave (CW). For an N-port array, the weight vector is [6]

$$\mathbf{w} = \frac{\mathbf{R}_x^{-1}\mathbf{c}}{\mathbf{c}^H\mathbf{R}_x^{-1}\mathbf{c}} \tag{1}$$

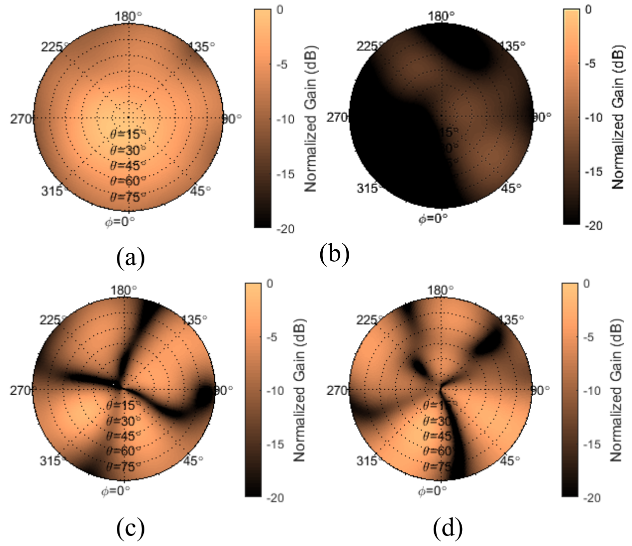

Figure 3. The measured normalized active gain patterns of array element in Fig. 1 (b). (a) $\boldsymbol{G_{1RHCP}}$ and (b) $\boldsymbol{G_{1LHCP}}$ when port 1 is active; and (b) $\boldsymbol{G_{2\theta}}$ and (c) $\boldsymbol{G_{2\varphi}}$ when port 2 is active.

where $\mathbf{R}_x \in \mathbb{C}^{N\times N}$ is the covariance matrix of the received signal, $\mathbf{c} \in \mathbb{C}^{N\times 1}$ is constraint vector which applies to the weight vector as $\mathbf{w}^H\mathbf{c} = \mathbf{1}$, and superscript H denotes the Hermitian operator. Further assuming uncorrelated desired signal, interference and noise, the covariance matrix can be written as

$$\mathbf{R}_x = \mathbf{R}_d + \mathbf{R}_i + \sigma^2\mathbf{I} \tag{2}$$

where $\mathbf{I}$ is the identity matrix, σ^2 is the noise power at the input of the adaptive array, and $\mathbf{R}_d$ and $\mathbf{R}_i$ are the desired signal and RFI covariance matrices, which for wide sense stationary CW signals at a single frequency are given by

$$\mathbf{R}_d = P_d\mathbf{u}_d\mathbf{u}_d^H \tag{3}$$

and

$$\mathbf{R}_i = \sum_{j=1}^{J} P_{ij}\mathbf{u}_{ij}\mathbf{u}_{ij}^H \tag{4}$$

respectively where P_d and P_i are desired signal and RFI powers at the input of the adaptive array. $\mathbf{u}_{d/i}$ is the array response vector for the desired or interference angle, given by

$$\mathbf{u}_{d/i} = \begin{bmatrix} \vec{E}_1(\theta_{d/i}, \varphi_{d/i}) \cdot \hat{e}_{d/i} \\ \vec{E}_2(\theta_{d/i}, \varphi_{d/i}) \cdot \hat{e}_{d/i} \\ \vdots \\ \vec{E}_N(\theta_{d/i}, \varphi_{d/i}) \cdot \hat{e}_{d/i} \end{bmatrix} \tag{5}$$

where $\vec{E}_n(\theta_{d/i},\varphi_{d/i}) = \sqrt{G_n(\theta_{d/i},\varphi_{d/i})}\,\hat{e}_a(\theta_{d/i},\varphi_{d/i})$ is the array realized gain multiplied by its polarization-phase vector when the n$^{\text{th}}$ port is active, and $\hat{e}_{d/i}$ is the polarization-phase vector of the desired or RFI plane wave. The SINR at the adaptive array output is given by

$$\mathrm{SINR_{out}} = \frac{\mathbf{w}^H \mathbf{R}_d \mathbf{w}}{\mathbf{w}^H(\mathbf{R}_i + \sigma^2 \mathbf{I})\mathbf{w}}. \tag{6}$$

The nulling performance of the array was studied using a Monte Carlo approach. A set of trials were run in MATLAB. In each trial J randomly polarized RFIs with powers 50 dB above noise level, are incident on the array from elevation angles between 0° to 30°. A desired signal is assumed to be 30 dB below noise level and the plane wave associated with it RHCP. The angle of incidence of the desired signal is swept in the upper hemisphere and using (6) the output SINR is computed for each angle. The available angular space is then defined as the region of the upper hemisphere with an output SINR above a threshold value.

Two different constraint vectors considered for the analysis are $\mathbf{c}_1 = [1\ 0 \ldots 0]^T$ and $\mathbf{c}_2 = \mathbf{u}_d$. The first constraint is equivalent to setting one of the weights equal to one, while the second is the directional constraint that ensures a unit gain in the direction of the incoming desired signal. The second constraint provides a higher SINR than the first constraint, but requires the knowledge of the incidence angle of the desired signal.

The performance of the proposed dual-mode array is compared to two other array types; A planar UCA and a spherical array both with nine CP TM_{11} elements as shown in Figure 4. The radii are chosen such that when taking into account the physical size of the TM_{11} patch, all of the arrays under study have the same footprint size on the x-y plane.

The results of the study averaged over 100 trials are shown in Figure 5. The angular available space is plotted against the threshold value of the output SINR, for different number of RFIs and the two different constraints for nulling. As seen, the proposed dual-mode array has better performance than the planar UCA, particularly when the constraint vector $\mathbf{c}_1$, corresponding to a blind null-steering (no knowledge of the satellite angles).

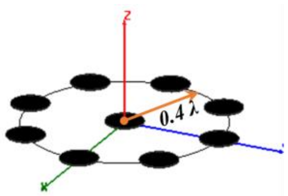

(a)

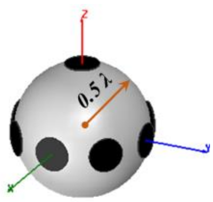

(b)

Figure 4. Two array configurations that are compared to the array of Figure 1. (a) Planar UCA of nine CP TM_{11} elements. (b) Spherical array of nine CP TM_{11} elements.

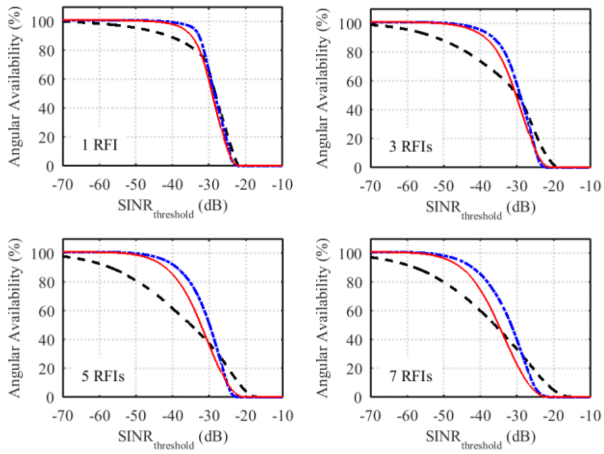

(a)

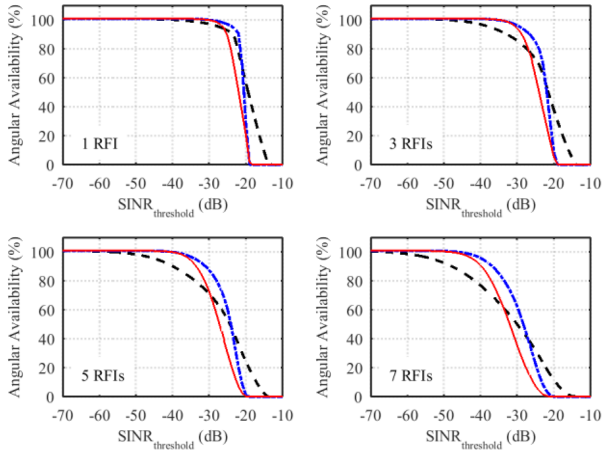

(b)

Figure 5. The angular available space with $\mathrm{SINR_{out}} > -35$ dB in the upper hemisphere for the proposed TM_{11}-TM_{21} array (———) compared to a planar UCA (— — —) and spherical array (—·—·—). (a) PMIN with $\mathbf{c}_1$. (b) PMIN with $\mathbf{c}_2$.

The actual angular availability will depend on the threshold value of the SINR that is required for the receiver to satisfy a certain value of carrier-to-noise ratio (C/N_0). For example, if an output SINR -35 dB is acceptable, Figure 6 shows the available angular space where reception is possible, plotted versus the number of RFIs. In Figure 6 (a), the constraint vector is $\mathbf{c}_1$, and in Figure 6 (b), the constraint vector is $\mathbf{c}_2$.

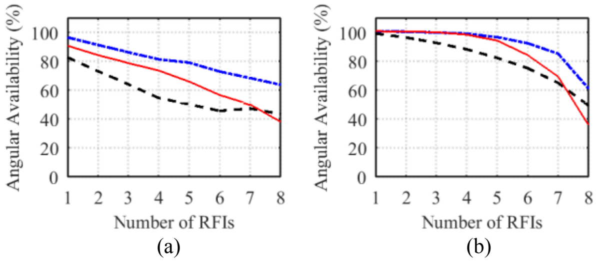

Figure 6. The angular available space with $\mathrm{SINR}_{out} > -35$ dB in the upper hemisphere for the proposed TM_{11}-TM_{21} array ( ) compared to a planar UCA (— — —) and spherical array ( ). (a) PMIN with $\mathbf{c_1}$. (b) PMIN with $\mathbf{c_2}$.

The radiation patterns of the arrays under study are given for a single trial in Figure 7, where four RHCP RFIs (white crosses) are incident on the arrays. The angle of the desired signal is marked by a blue dot. It can be observed in this example that the nulls formed in the planar UCA are stretched along the elevation plane (Figure 7 (a)) while this effect is less severe in the dual-mode array (Figure 7 (c)).

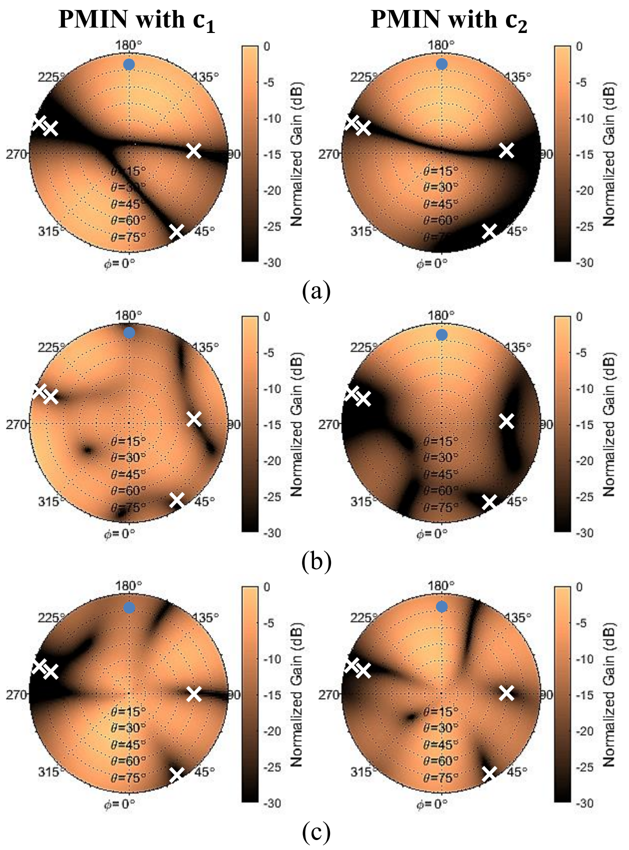

Figure 7. The normalized array gain pattern after nulling using PMIN with constraint vectors $\mathbf{c_1}$ (left column) and $\mathbf{c_2}$ (right column). (a) The planar UCA in Figure 4. (b) The spherical array in Figure 4. (c) The dual-mode array in Figure 1.

4. Conclusions

The second azimuthal mode of the circular MSA was used to improve the angular coverage of a planar CRPA. An array of dual-mode TM_{11}-TM_{21} mode elements was designed and its nulling performance was evaluated. It was shown that the proposed array has a better angular availability for near-horizon randomly polarized interferes, compared to a planar UCA of TM_{11} elements.

5. References

1. C. Fernández-Prades, J. Arribas and P. Closas, "Robust GNSS Receivers by Array Signal Processing: Theory and Implementation," in *Proceedings of the IEEE*, vol. 104, no. 6, pp. 1207-1220, June 2016. doi: 10.1109/JPROC.2016.2532963.

2. G. Byun, H. Choo and S. Kim, "Improvement of Pattern Null Depth and Width Using a Curved Array With Two Subarrays for CRPA Systems," in *IEEE Transactions on Antennas and Propagation*, vol. 63, no. 6, pp. 2824-2827, June 2015, doi: 10.1109/TAP.2015.2416758.

3. B. R. Rao, W. Kunysz, R. Fante, and K. McDonald, GPS/GNSS Antennas. Norwood, MA, USA: Artech House, 2013.

4. I. J. Gupta *et al.*, "Non-Planar Adaptive Antenna Arrays for GPS Receivers," in *IEEE Antennas and Propagation Magazine*, vol. 52, no. 5, pp. 35-51, Oct. 2010, doi: 10.1109/MAP.2010.5687504.

5. N. R. Labadie, S. K. Sharma and G. M. Rebeiz, "A Circularly Polarized Multiple Radiating Mode Microstrip Antenna for Satellite Receive Applications," in *IEEE Transactions on Antennas and Propagation*, vol. 62, no. 7, pp. 3490-3500, July 2014, doi: 10.1109/TAP.2014.2320860.

6. R. A. Monzingo and T. W. Miller, Introduction to Adaptive Arrays. New York Wiley, 1980.